Automated Laboratory Kilogram-Scale Graphene Production from Coal

Lucas Eddy,[1,2] Duy Xuan Luong,[1,2,3] Jacob L. Beckham,[2] Kevin M. Wyss,[2] Tyler J. Cooksey,[3] Phelecia Scotland,[4] Chi Hun Choi,[4] Weiyin Chen,[2] Paul A. Advincula,[2] Zhiyong Zhang,[3] Vladimir Mancevski,[2] Carter Kittrell,[2] Yimo Han,[4] and James M. Tour[2,4,5,6]*

[1]Applied Physics Graduate Program and Smalley-Curl Institute, [2]Department of Chemistry, [3]Universal Matter Inc., Houston, 900 S Loop W Suite 175, Houston, TX 77054, [4]Department of Materials Science and NanoEngineering, [5]The NanoCarbon Center and The Rice Advanced Materials Institute, and [6]Department of Computer Science, Rice University, 6100 Main Street, Houston, Texas 77005, United States

*Corresponding Author (Emails: tour@rice.edu)

Key words: graphene, flash Joule heating, life cycle assessment, kilogram-scale, automation

Abstract: The flash Joule heating (FJH) method converts many carbon feedstocks into graphene in milliseconds to seconds using an electrical pulse. This opens an opportunity for processing low or negative value resources, such as coal and plastic waste, into high value graphene. Here, we demonstrate a lab-scale automation FJH system that allows the synthesis of 1.1 kg of turbostratic flash graphene from coal-based metallurgical coke (MC) in 1.5 h. The process is based on the automated conversion of 5.7 g of MC per batch using an electrical pulse width modulation system to conduct the bottom-up upcycle of MC into flash graphene. We then compare this method to two other scalable graphene synthesis techniques by both a life cycle assessment and a technoeconomic assessment.

1. Introduction

The high-yield bottom-up production of graphene, such as by chemical vapor deposition, has typically been limited to submilligram or milligram scales. The flash Joule heating (FJH) method provides a remedy to this through its capability to convert virtually any solid carbon

source into turbostratic flash graphene (FG) by a reaction completed in milliseconds or seconds.[1-11] This is performed by discharging a kilojoule-scale electrical pulse through a carbon feedstock to rapidly Joule heat the reactants. The versatility of FJH also permits the synthesis of inorganic complexes,[12-14] the extraction of metals from industrial waste,[15,16] and the ultrafast synthesis of various carbon compounds.[17,18] The conversion and morphology of the synthetic products depend on the heating profile as determined by the electrical discharge rate.[19] In FG synthesis, this heating profile has a significant effect on the turbostraticity and sheet diameter.[20] The FG quality is controlled by the rate and duration of discharge of the capacitors making up the FJH system. Furthermore, constraints on the rate at which FJH can be performed are imposed by both the charging rate of the capacitor banks as well as the automation feed rate.

The scale of the synthesis of FG is limited by several factors, including the energy capacity of the FJH used, the sample loading and unloading rate, and the reduction in product uniformity as the volume of the reaction tube increases. The energy required to convert an amorphous carbon feedstock to 1 g of FG has been previously reported as 10-23 kJ, based on the input feedstock type.[5,6] The energy efficiency of this process is also reduced by the requirement of 1-5 low-voltage flash "pretreatments" that are typically performed on flashing feedstocks to both reduce their resistivity and the presence of volatiles prior to the main, high voltage flash.

This work describes an approach by which the electrical current profile of the capacitor bank discharge can be tuned by pulse-width modulation (PWM) to improve FG quality and uniformity and to eliminate or reduce the need for multiple flashing pretreatments, allowing FG to be produced with greater energy efficiency. We also discuss the implementation of an automated system that loads the FJH reactor with a reaction vessel, charges the capacitor banks, flashes, and unloads the reacted vessel, independent of constant human input, allowing for kilogram-scale FG synthesis.

2. Results and Discussion

2.1. Scaling Up

For the first two years since the discovery of the FJH process in 2018, the FG production rate had, on average, doubled each 9 weeks **(Figure 1a)**. The exponential growth in production rate resulted due to two factors: building a reactor for the higher capacity flashing system that is capable of flashing 10 g of metallurgical coke (MC) in each batch **(Figure 1b)**, and the automated sample reloading system **(Figure 1c)**. The FJH system **(Figure S1)** is powered by 48 capacitors for a total of 0.624 F capacitance. Each set of 8 capacitors are put into a capacitor bank and controlled by a solid-state relay. Six capacitor banks are connected to the kill switch upstream from the connection to the sample holder. To slow the current for more stable electrical control, a 0.3 μH inductor is put in series with the circuit. The sample can be flashed either in a controlled environment flashing chamber or in ambient atmosphere; there is sufficient outgassing from the sample to protect it from combustion in air.

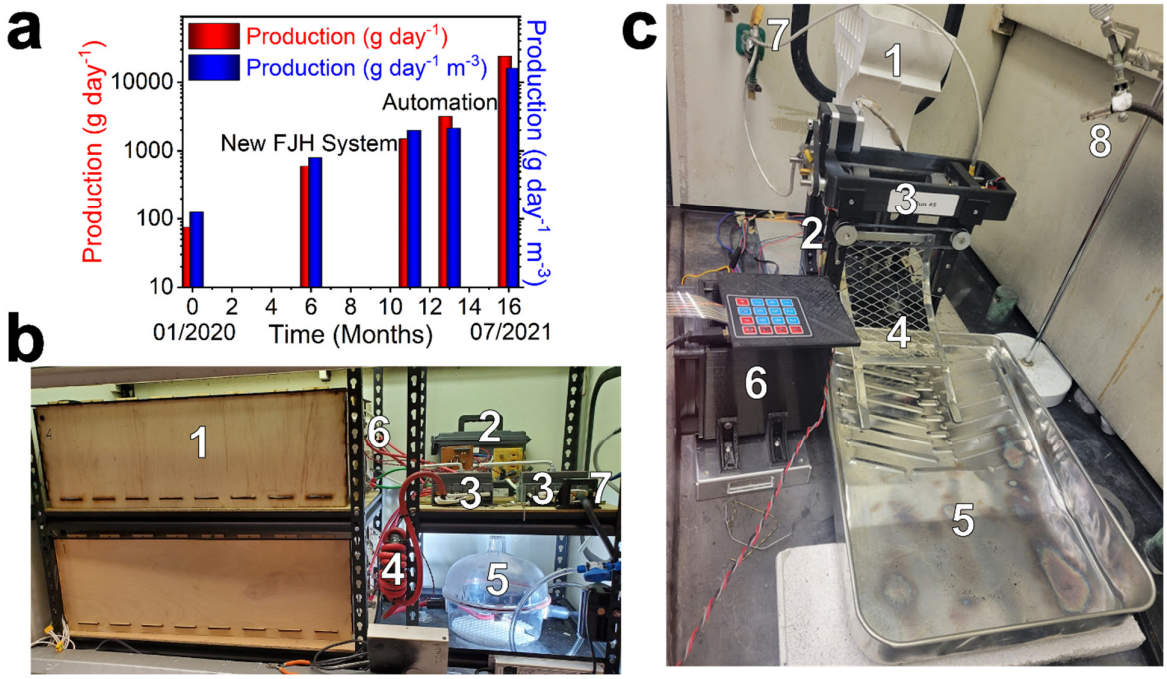

Figure 1. a) Production rate increases during the first two years of carbon materials conversion using the FJH process both as a function of grams of graphene per day and as a function of

grams of graphene per day per cubic meter of fume hood space. b) The scale-up flashing system that has total capacitance of 0.624 F with 500 V DC rating and is capable of flashing 10 g of MC per batch. b1: Six capacitor banks, each consisting of eight 13 mF capacitors in parallel. b2: Switching controller that controls the simultaneous discharge of the capacitor banks. b3: Kill switches to toggle the flashing system. b4: Inductor that slightly slows the discharge rate by raising the time constant. b5: Flashing chamber to contain sample outgassing. c) The automated system can flash 5.7 g of MC per batch, reload the new sample, and charge the capacitor banks all within ~20 s per cycle. Most of this time is spent recharging the capacitors. c1: The magazine that holds the MC-filled quartz tube reaction vessels prior to flashing. c2: The stand for the flashing chamber. c3: The 3D-printer reaction vessel holder that loads, flashes, and unloads reaction vessels. c4: The ramp onto which the reacted quartz tube reaction vessels drop upon being unloaded. c5: The basin used to collect flashed samples. c6: The controller for the loading and unloading systems. c7: The connection to the 0.624 F capacitor banks located in the opposite hood seen in b. c8: An air hose for cooling the reaction vessel to mitigate the melting of the 3D printed plastic flashing stand.

The automated system is controlled by a customized LabVIEW program. Once the flashing sample is loaded inside the flashing reaction vessel **(Figure S2a)**, the FJH system will commence the flash. Each sample is comprised of 5.7 g metallurgical coke loaded into a quartz tube with fritted graphite electrodes on the outside **(Figure S2b)**. After the flash is done, the sample is dropped into a collection tray made from a paint roller pan, and the new sample is automatically loaded into the reaction vessel holder. The graphite electrodes and the quartz tubes can be reused for subsequent flashes **(Figure S2c)**. The time required for charging the capacitor banks and flashing the samples is significantly less than the time required to prepare the samples **(Figure S3)**.

A positive correlation is found between the flashing voltage and FG quality **(Figure S4)**. The quality of the FG **(Figure S4a)** and the Raman map spectra **(Figure S4b)** of the FG produced as part of the 1 kg collective product are indications that the production was successful. The FG was confirmed to be turbostratic by the presence of the turbostratic TS_1 and TS_2 Raman spectroscopic peaks **(Figure S5)**, and the missing M band at ~1750 cm^{-1}.

2.2. Flashing with Pulse Width Modulation

Pulse width modulation (PWM, **Figure 2)** using a variable frequency driver (VFD) is used to cut the continuous discharge of the capacitor banks into sections *via* the rapid (1 kHz) on-and-off switching enabled by insulated-gate bipolar transistors (IGBTs) mounted on each capacitor bank. A customized LabVIEW program controls the frequency of IGBT switching; this is the fraction of time that the switch is turned on (duty cycle), as well as the duration of each duty cycle. Thus, to compensate for the exponential decrease in power during the discharge of a capacitor, higher duty cycles are selected as the reaction proceeds to maintain near-constant electrical power over the duration of the discharge, as seen in **Figure 2a**.

With only a DC flash, the single current spike results in measured surface temperatures significantly higher than for an equivalent flash using PWM. This rapid temperature increase models more closely an adiabatic process and increases the risk of violent outgassing that could break the reaction vessel. As a precaution against this, two lower voltage “pretreatment” DC flashes (150 V for 500 ms here) are performed prior to the primary, high voltage DC flash. As seen in **Figure 2a**, the final DC flash has a peak current of >1500 A. With a PWM flash however, the pretreatments are not necessary, and the peak current is less than 1000 A, reducing the flashing time and the risk of vessel and equipment failure, while increasing the energy efficiency and production throughput.

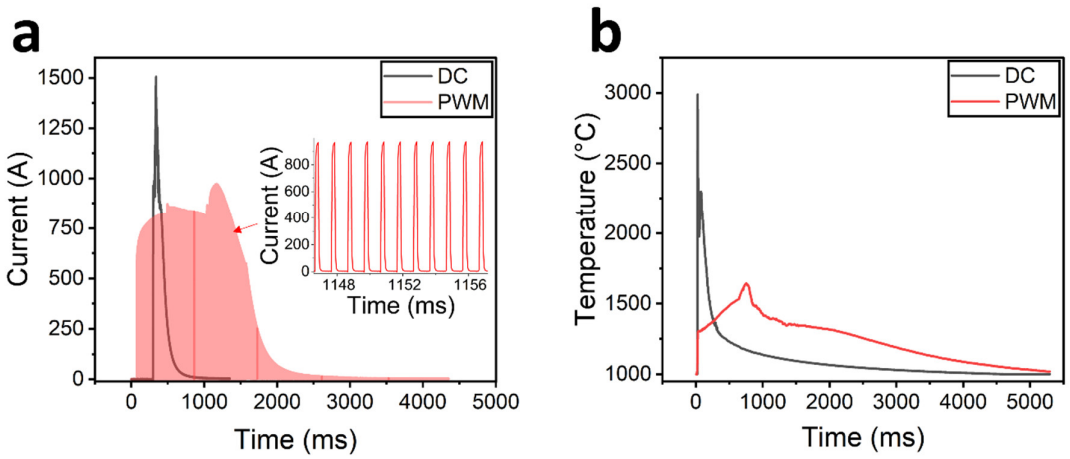

Figure 2. Reaction conditions of PWM compared to direct DC flashes. a) Current profile of a 330 V DC flash *vs* a 330 V PWM flash. The pulse sequence of the second-time scale PWM flash (red area) is magnified to the millisecond-time scale in the inset as a single pulse being divided into 1 kHz duty cycles (sharp red peaks) to reduce the average power used. The energies of the DC and PWM flashes are the same. b) Temperature profile of the same DC and PWM flash as measured using a Micro-Epsilon CTRM1H1SF100-C3 pyrometer.

The temperature profile shows that the DC flash reaches 3000 °C and has a <500 ms duration, matching well with the result from our previous publication.[6] The PWM flash barely exceeds 1850 °C on the surface, but has duration of ~2 s **(Figures 2 and S6-S7)**. However, when comparing the graphene quality by Raman analysis, the two products are spectroscopically similar **(Figure 3)**, indicating that the lower temperature can be replaced by a longer flashing time. Even though the DC flash has a shorter duration, the production throughput using DC is much lower than that using PWM flash conditions because of the addition of lower-voltage pretreatment flashes. PWM also allows for sustaining a desired flashing temperature ± 200 °C for several seconds **(Figure S8)**.

2.3. Characterization of FG

Raman spectroscopy is one of the primary tools used to evaluate graphene quality, as shown in **Figure 3**. In particular, the ratio of the D, G, and 2D graphene peaks are used as a comparison. The D/G Raman intensity ratio is correlated to graphene lattice defect density and is inversely correlated to graphene sheet size and thus graphene quality. The 2D/G Raman intensity ratio is positively to graphene conversion. As seen in **Figure 3a**, PWM-MC-FG has a comparable D/G ratio as MC-FG produced from an unmodulated DC flash, and both have smaller ratios than commercial graphene nanoplatelets, indicating lower defect density in the FG. In **Figure 3b**, PWM-MC-FG is shown to have a higher 2D/G ratio than MC-FG, suggesting better graphene quality. Finally, PWM also leads to improved graphene quality that compares favorably to MC-FG. This is an essential improvement since scaling up without PWM can lead to reductions in product uniformity.

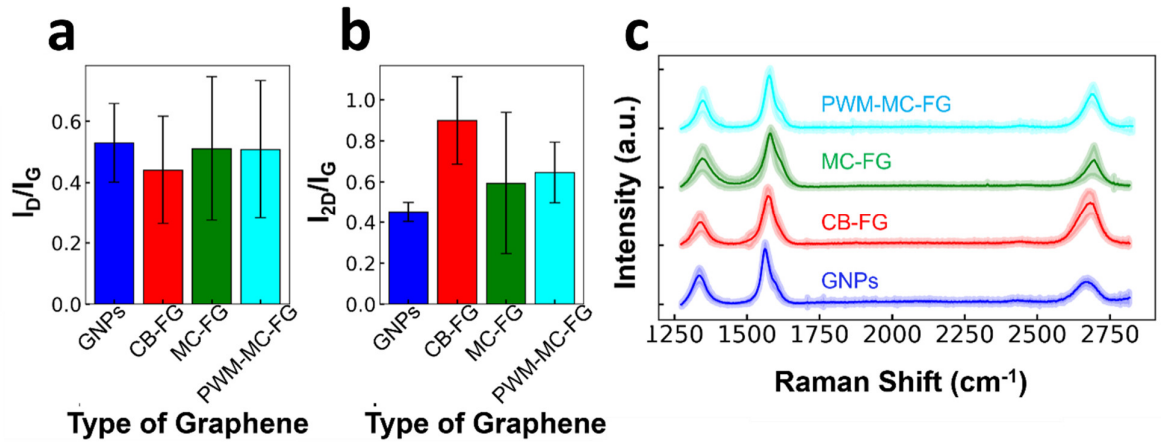

Figure 3. a) Comparison of the ratio of the intensities of the D and G Raman bands for FG from different graphene products, including commercial graphene nanoplatelets (GNP), carbon black-derived flash graphene (CB-FG) from a DC flash, metallurgical coke-derived flash graphene from an unmodulated DC flash (MC-FG) and pulse width modulation produced metallurgical coke-derived flash graphene (PWM-MC-FG). b) Comparison of the ratio of the intensities of the 2D and G Raman bands for different carbon feedstocks. The ratio of the

amplitude of the D Raman peak to the G Raman peak is inversely proportional to the graphene sheet size. c) Comparison of Raman maps of each of the feedstocks. The standard deviation of the 200 scans across 100 points on each sample is expressed as shaded areas around the main lines. Batches were mixed to ensure uniformity prior to Raman analysis. The scanning electron microscopy (SEM) and x-ray diffraction (XRD) analyses are also consistent with high graphene quality **(Figures S9-S10)**.

Dispersion tests using water-surfactant shown in **Figure 4** demonstrate that MC-FG and CB-FG from PWM flashing has dispersibility consistent with previous results for FG.[21-23] The source of dispersibility of FG was found to be dependent on the surface area of the feedstock used. MC-FG was found to have a surfactant enhanced dispersibility of 0.15 g/L while CB-FG has dispersibility of ~3 g/L, which is superior to that of most commercial graphene.[6] Transition electron microscopy (TEM) images confirm that the graphene crystalline quality remains high, even while being mass-produced through automation.

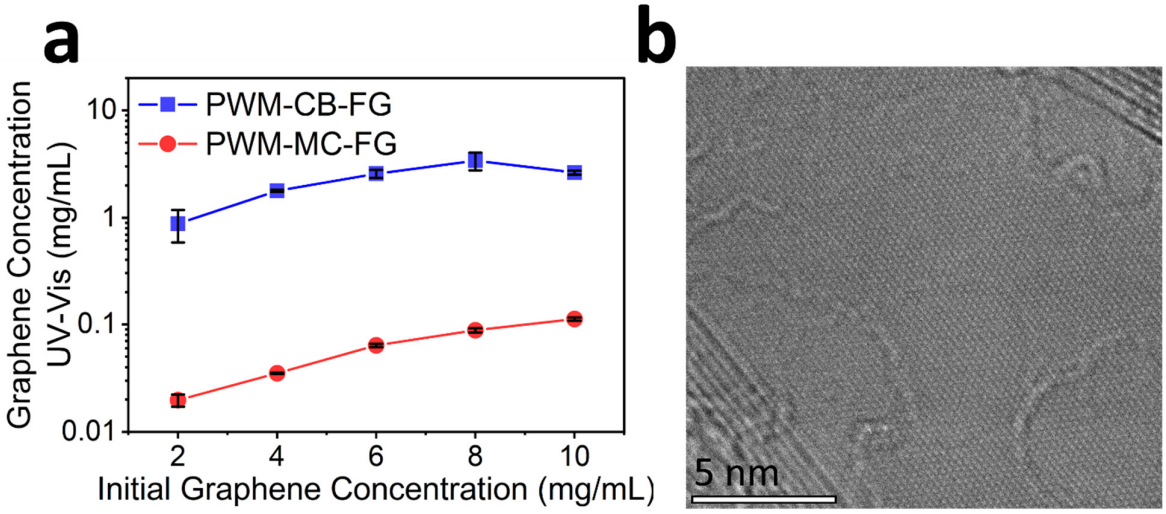

Figure 4. a) UV-Vis dispersion map of FG concentration from a 5.7 g MC feedstock prepared at 370 V using PWM flash conditions compared to PWM-CB-FG flashed with same

energy/mass ratio. The FG dispersions were prepared in aqueous 1% Pluronic (F-127) that was subsequently bath sonicated. While MC-FG disperses poorly due to the low surface area of MC, the PWM-CB-FG, since CB has a higher surface area, disperses better than commercial graphene.[6] b) TEM image of this PWM-MC-FG feedstock with the same parameters.

The ability to perform flashing with a tunable and more uniform heating profile enables consecutive flashes to be performed without concern for significant variance in product quality between flashes. This was essential for the addition of an automated extension to the FJH system, as shown in **Figure 1c**. This system automatically loads the reaction vessel, charges the capacitor banks, flashes the material in the reaction vessel, and unloads the reaction vessel before repeating. With the automated system, batches were run at different flashing voltages yielding over 200 samples in total, amounting to 1.1 kg of FG in 1.5 h **(Movie S1 and S2)**. Raman spectroscopy shows a positive correlation between the FG yield and the energy input into the samples, as shown in **Figure S4**, allowing a yield of >90% for the highest voltage batch, which indicates good carbon feedstock conversion. The current rate of flashing permits over 10 kg of FG to be produced per day.

In addition to allowing a more time-efficient reaction, scaling up reduces the energy required per g of reactant. This is largely due to the flashing geometry, since the 0.57 g flash is performed in an 8 mm diameter, 4 cm length tube, whereas the 5.7 g flash is performed in a 16 mm diameter, 8 cm length tube. Consequently, the smaller tube has a higher surface area to volume ratio, permitting more rapid heat loss. Scaling up one order of magnitude to this larger batch size reduces the energy requirement of flashing by up to 40 % **(Figure 5)**.

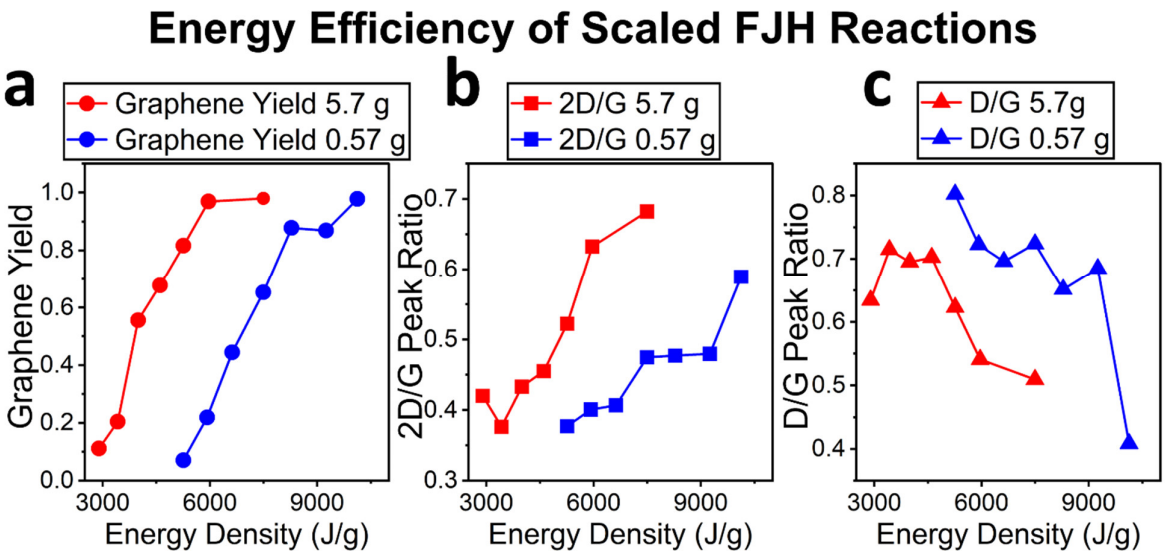

Figure 5. Comparison of graphene quality between 0.57 g and 5.7 g flash loadings *via* a comparison of a) graphene yield b) 2D/G Raman peak ratio and c) D/G Raman peak ratio. Less energy is required to obtain the same flash graphene quality as the reaction scale increases. Each data point is determined from the average of a square map of 200 Raman scans across 1 mm^2 of sample. The graphene yield is calculated by first selecting all the scans with an observed G band and then among these, counting all the individual Raman scans with a 2D/G peak ratio of at least 0.3 and dividing this by the total number of G-band scans.

2.4. Life Cycle and Technoeconomic Assessments

The mass scales that flash Joule heating can achieve are comparable to those achieved by previously existing and scalable top-down synthesis procedures. Graphene manufacturing by exfoliation of graphite or by reducing graphene oxide produced by Hummer's method have been extensively covered in the literature. All three methods can produce similar powdered graphene of size and quality appropriate to implement in composites. In contrast to flash Joule

heating, both other methods are solvent-intensive and require hours of processing per batch. This raises the energy, resource cost, and toxicity profile significantly.

A cradle-to-gate life cycle assessment (LCA), and a cradle-to-gate technoeconomic assessment (TEA) were performed comparing the synthesis of graphene via flash Joule heating to those of exfoliation and reduction-produced graphene, following a previous LCA on the latter two.[24] The scope, inputs, and assumptions are categorized in the supporting information **(Figures S11-S17)**. A full spreadsheet of values used is also included. The results of these assessments are shown in **Figure 6**.

The flash graphene process scaled here requires that metallurgical coke chunks are first ground to several millimeters in diameter before being filled in a quartz reaction vessel and flashed. Since the reaction vessels and electrodes are reusable, they are not considered in these assessments. The energy cost of graphene is at 14 MJ/kg, most of which comes from the flashing itself. This compares to 470 MJ/kg cost of graphene derived from ultrasonication-based exfoliation and 970 MJ/kg cost of graphene from reduced graphene oxide produced from Hummers' process, though the last of these can be made slightly more efficient with an optimized ratio of solvents.[25] Paton et. al. also presented a method for scalable production of graphene, demonstrating the synthesis of 20 g graphene in 4 h by shear-mixing.[26] Though we present the LCA and TEA of this process in **Figures S18-S20**, the yield of this scaled-process was only 0.07%, and the resulting product among this low yield exhibited incomplete exfoliation. Consequently, the price difference between flash graphene and graphene from these two other methods are significant. Flash graphene can be made at $0.16/kg ($160/tonne), most of which comes from the cost of the metallurgical coke feedstock. Ultrasonication-derived was determined to cost $44/kg to produce, while graphene from reduced graphene oxide costs

significantly more at $3600/kg. Given the current price of graphene at ~ $50/kg, flash Joule heating has great promise to be widely used in the industrial sector.

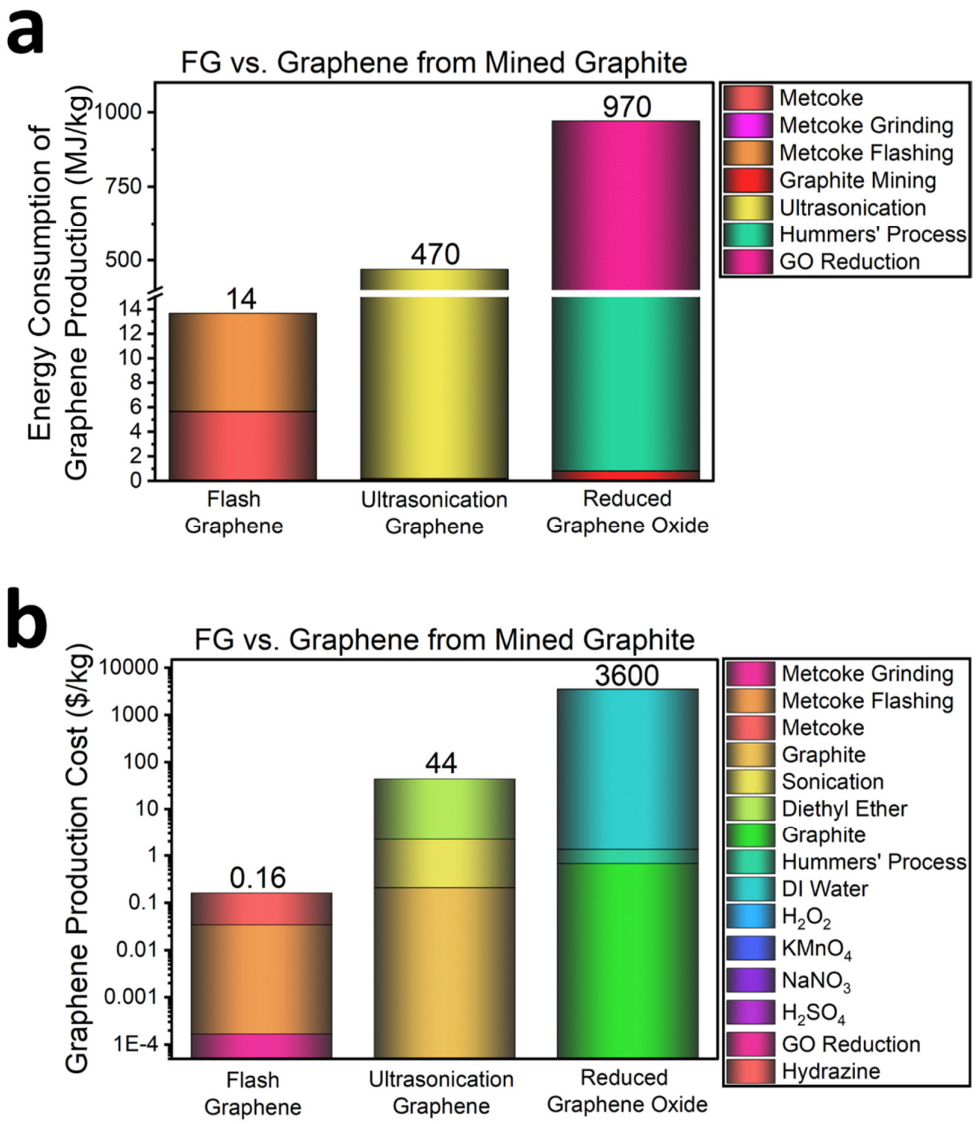

Figure 6. a) Results of life cycle assessment comparing the scaled flash graphene method with that of two different scalable methods for producing graphene from graphite exfoliation. b) Results of the technoeconomic assessment comparing the same processes. Some quantities are too small to be clearly visible in the graphs.

3. Conclusion

In summary, the implementation of PWM enables enhanced control of the electric discharge of the FJH system's capacitor banks. This allows for control over the heating profile during FG synthesis, enabling flashes to be optimized around individual feedstocks. The increase in consistency that PWM allows consecutive flashes to be performed by the automated system without significant variance in graphene quality. Further, scale-up reduces the power demand in the FJH process. These innovations make flash Joule heating a more cost and energy efficient method of scalable graphene synthesis.

4. Methods/Experimental Section

4.1. Flash Graphene Synthesis

Materials: Metallurgical coke obtained from SunCoke was ground and sieved until particle diameter was between 0.8- and 2-mm. Additional characterization of this raw metallurgical coke is shown in **Figure S21**.

FJH System: The circuit diagram of the flash Joule heating system is shown in **Figure S1** of the Supplementary Information. The automated system uses the same discharge source as that presented in previous literature. The capacitors were charged to 370 V prior to each flash, which translates to 15 kJ of energy per g of MC reacted. The 1.1 kg FG produced *via* automation was performed across four sessions totaling 90 minutes.

PWM was implemented using a custom written LabVIEW program with a frequency of 1000 Hz. The duty cycle of the PWM was after some optimization programmed to be 10% for 1 s, 20% for 0.5 s, and 50% for 5 s before dropping to 0%.

4.2. Graphene Dispersion

Pluronic (F127) is a triblock copolymer of polyethylene glycol-polypropylene glycol-polyethylene glycol used in the dispersion tests in **Figure 4** was purchased from Millipore

Sigma. F127 is a non-ionic copolymer powdered surfactant with a chemical formula of $(C_3H_6O \cdot C_2H_4O)_x$. A solution consisting of 1 wt% of Pluronic (F127) was prepared to aid in the dispersion of graphene. Yan et al. showed that F127 adsorbs to the surface of graphene oxide in an "anchor-buoy-type configuration."[27] Subsequently, long ethylene oxide (EO) segments of F127 were extended into the water to form a hydration protective layer, effectively inhibiting the aggregation of GO sheets. A similar phenomenon can be observed in the dispersion of graphene.

4.3. Life Cycle and Technoeconomic Assessments

A cradle-to-gate life cycle assessment considers the energy and materials cost of a process from the production of the raw materials all the way to the synthesis of the final product, in addition to the environmental impacts of this process. A cradle-to-gate technoeconomic analysis analyzes the monetary costs associated with these steps. The objectives of these two assessments were to compare the resource and monetary costs and environmental impacts of flash graphene to that of two other scaled-up graphene synthesis methods. This system focuses primarily on three steps in the life cycle: raw material production, reactant preparation, and the graphene synthesis reaction. The costs related to the transportation of raw materials were not considered in these assessments. The functional unit considered here was 1 kg of high purity graphene. This high purity threshold was set at >97% conversion for flash graphene. **Figures S11-S17** discuss the details of these assessments further. The results of a brief survey of commercial graphene production techniques are given in **Table S1.**

4.4. Characterization and Measurements

Raman spectra were collected using a Renishaw Raman microscope equipped with a 532 nm laser and LiveTrack software to automatically adjust focus between spectra. A 50x objective lens was used to collect all spectra. Custom Python scripts were used to analyze the Raman spectral mapping data and identify the presence and intensity of the D, G, and 2D graphene

peaks in order to calculate the graphene yield. Sample points exhibiting a 2D/G peak ratio of at least 0.3 were counted as graphene in the graphene yield calculation. 2D/G peak ratios below this were considered unconverted and thus factored into the yield calculation. Scans for which the G peak could not be identified were not included in the final graphene yield calculation due to the scan being poorly focused. Each Raman spectrum displayed and each peak ratio and yield calculated is done so from the average of 100 points across a 1 mm^2 area of the sample, with 2 scans being averaged together at each point. Samples are crushed and mixed in a mortar and pestle prior to scanning. Powder XRD data was collected on a Rigaku SmartLab X-ray Diffractometer using a Cu X-ray tube. SEM images were taken with an FEI Quanta 400 ESEM FEG. TEM images were obtained with an FEI Titan Themis3.

Supporting Information

Supporting Information is available from the Wiley Online Library.

Acknowledgements The funding of the research was provided by the DOE-NETL (DE-FE0031794, J.M.T.) and the U.S. Army Corps of Engineers, ERDC (W912HZ-21-2-0050, J.M.T.). The characterization equipment used in this project is partly from the Shared Equipment Authority (SEA) at Rice University.

Disclosures—Conflict of Interest

Rice University owns intellectual property on the flash Joule heating strategy. J. M. T. and D. X. L. are stockholders in Universal Matter Ltd., a company that has licensed the intellectual property from Rice University. J. M. T. is not an officer or director in Universal Matter Ltd. D.X.L. contributions occurred when he was employed solely by Rice University. He has subsequently been employed by Universal Matter Ltd. All conflicts of interest are managed through regular disclosure to the Rice University Office of Sponsored Programs and Research Compliance.

References

[1] K. M. Wyss, J. T. Li, P. A. Advincula, K. V. Bets, W. Chen, L. Eddy, K. J. Silva, J. L. Beckham, J. Chen, W. Meng, B. Deng, S. Nagarajaiah, B. I. Yakobson, J. M. Tour. *Adv. Mater.* 2023, **35**, 2209621.

[2] K. M. Wyss, J. L. Beckham, W. Chen, D. X. Luong, P. Hundi, S. Raghuraman, R. Shahsavari, J. M. Tour. *Carbon* 2021, **174**, 430-438.

[3] P. A. Advincula, D. X. Luong, W. Chen, S. Raghuraman, R. Shahsavari, J. M. Tour. *Carbon* 2021, **178**, 649-656.

[4] K. M. Wyss, Z. Wang, L. B. Alemany, C. Kittrell, J. M. Tour. *ACS Nano* 2021, **15**, 10542-10552.

[5] W. A. Algozeeb, P. E. Savas, D. X. Luong, W. Chen, C. Kittrell, M. Bhat, R. Shahsavari, J. M. Tour. *ACS Nano* 2020, **14**, 15595-15604.

[6] D. X. Luong, K. V. Bets, W. A. Algozeeb, M. G. Stanford, C. Kittrell, W. Chen, R. V. Salvatierra, M. Ren, E. A. McHugh, P. A. Advincula, Z. Wang, M. Bhatt, H. Guo, V. Mancevski, R. Shahsavari, B. I. Yakobson, J. M. Tour. *Nature* 2020, **577**, 647-651.

[7] G. Chen, Y. Wang, X. Wang, Y. Zhao, Q. Dong, L. Hao, M. Hong, M. Guo, H. Qiao, W. Xiong, L. Hu. *ACS Mater. Lett.* 2022, **4**, 480-486.

[8] W. Chen, C. Ge, J. T. Li, J. L. Beckham, Z. Yuan, K. M. Wyss, P. A. Advincula, L. Eddy, C. Kittrell, J. Chen, D. X. Luong, R. A. Carter, J. M. Tour. *ACS Nano* 2022, **16**, 6646-6656.

[9] P. A. Advincula, V. Granja, K. M. Wyss, W. A. Algozeeb, W. Chen, J. L. Beckham, D. X. Luong, C. F. Higgs, J. M. Tour. *Carbon* 2023, **203**, 876-885.

[10] P. A. Advincula, W. Meng, L. J. Eddy, J. L. Beckham, I. R. Siqueira, D. X. Luong, W. Chen, M. Pasquali, S. Nagarajaiah, J. M. Tour. *Macromol. Mater. Eng.* 2023, **308**, 2200640.

[11] K. Sattari, L. Eddy, J. L. Beckham, K. M. Wyss, R. Byfield, L. Qian, J. M. Tour, J. Lin. *Digital Discovery* 2023, **2**, 1209-1218.

[12] C. Wang, W. Ping, Q. Bai, H. Cui, R. Hensleigh, R. Wang, A. H. Brozena, Z. Xu, J. Dai, Y. Pei, C. Zheng, G. Pastel, J. Gao, X. Wang, H. Wang, J.-C. Zhao, B. Yang, X. Zheng, J. Luo, Y. Mo, B. Dunn, L. Hu. *Science* 2020, **368**, 521-526.

[13] W. Chen, Z. Wang, K. V. Bets, D. X. Luong, M. Ren, M. G. Stanford, E. A. McHugh, W. A. Algozeeb, H. Guo, G. Gao, B. Deng, J. Chen, J. T. Li, W. T. Carsten, B. I. Yakobson, J. M. Tour. *ACS Nano* 2021, **15**, 1282-1290.

[14] Q. Dong, M. Hong, J. Gao, T. Li, M. Cui, S. Li, H. Qiao, A. H. Brozena, Y. Yao, X. Wang, G. Chen, J. Luo, L. Hu. *Small* 2022, **18**, 2104761.

[15] B. Deng, X. Wang, X. Luong Duy, A. Carter Robert, Z. Wang, B. Tomson Mason, M. Tour James. *Sci. Adv.* 2022, **8**, eabm3132.

[16] B. Deng, D. X. Luong, Z. Wang, C. Kittrell, E. A. McHugh, J. M. Tour. *Nat. Commun.* 2021, **12**, 5794.

[17] B. Deng, Z. Wang, W. Chen, J. T. Li, D. X. Luong, R. A. Carter, G. Gao, B. I. Yakobson, Y. Zhao, J. M. Tour. *Nat. Commun.* 2022, **13**, 262.

[18] W. Chen, R. V. Salvatierra, J. T. Li, C. Kittrell, J. L. Beckham, K. M. Wyss, N. La, P. E. Savas, C. Ge, P. A. Advincula, P. Scotland, L. Eddy, B. Deng, Z. Yuan, J. M. Tour. *Adv. Mater.* 2023, **35**, 2207303.

[19] W. Chen, J. T. Li, Z. Wang, W. A. Algozeeb, D. X. Luong, C. Kittrell, E. A. McHugh, P. A. Advincula, K. M. Wyss, J. L. Beckham, M. G. Stanford, B. Jiang, J. M. Tour. *ACS Nano* 2021, **15**, 11158-11167.

[20] M. G. Stanford, K. V. Bets, D. X. Luong, P. A. Advincula, W. Chen, J. T. Li, Z. Wang, E. A. McHugh, W. A. Algozeeb, B. I. Yakobson, J. M. Tour. *ACS Nano* 2020, **14**, 13691-13699.

[21] Y. Xu, H. Cao, Y. Xue, B. Li, W. Cai. *Nanomater.* 2018, **8**,

[22] A. O'Neill, U. Khan, P. N. Nirmalraj, J. Boland, J. N. Coleman. *J. Phys. Chem. C* 2011, **115**, 5422-5428.

[23] L. Dong, Z. Chen, X. Zhao, J. Ma, S. Lin, M. Li, Y. Bao, L. Chu, K. Leng, H. Lu, K. P. Loh. *Nat. Commun.* 2018, **9**, 76.

[24] R. Arvidsson, D. Kushnir, B. A. Sandén, S. Molander. *Environ. Sci. Technol.* 2014, **48**, 4529-4536.

[25] D. C. Marcano, D. V. Kosynkin, J. M. Berlin, A. Sinitskii, Z. Sun, A. Slesarev, L. B. Alemany, W. Lu, J. M. Tour. *ACS Nano* 2010, **4**, 4806-4814.

[26] K. R. Paton, E. Varrla, C. Backes, R. J. Smith, U. Khan, A. O'Neill, C. Boland, M. Lotya, O. M. Istrate, P. King, T. Higgins, S. Barwich, P. May, P. Puczkarski, I. Ahmed, M. Moebius, H. Pettersson, E. Long, J. Coelho, S. E. O'Brien, E. K. McGuire, B. M. Sanchez, G. S. Duesberg, N. McEvoy, T. J. Pennycook, C. Downing, A. Crossley, V. Nicolosi, J. N. Coleman. *Nat. Mater.* 2014, **13**, 624-630.

[27] Y. Yan, L. Piao, S.-H. Kim, W. Li, H. Zhou. *RSC Adv.* 2015, **5**, 40199-40204.